SLAC-PUB-14369
SU-ITP-11/03

Jet Dipolarity: Top Tagging with Color Flow

Anson Hook,[1,2] Martin Jankowiak,[1,2] and Jay G. Wacker[1]

[1] *Theory Group, SLAC, Menlo Park, CA 94025*
[2] *Physics Department, Stanford University, Stanford, CA 94305*

A new jet observable, dipolarity, is introduced that can distinguish whether a pair of subjets arises from a color singlet source. This observable is incorporated into the `HEPTopTagger` and is shown to improve discrimination between top jets and QCD jets for moderate to high p_T.

Introduction

The impressive resolution of the ATLAS and CMS detectors means that a typical QCD jet at the LHC deposits energy in $\mathcal{O}(10-100)$ calorimeter cells. Such fine-grained calorimetry allows for jets to be studied in much greater detail than previously, with sophisticated versions of current techniques making it possible to measure more than just the bulk properties of jets (*e.g.* event jet multiplicities or jet masses). One goal of the LHC is to employ these techniques to extend the amount of information available from each jet, allowing for a broader probe of the properties of QCD. The past several years have seen significant progress in developing such jet substructure techniques. A number of general purpose tools have been developed, including: (i) top-tagging algorithms designed for use at both lower [1, 2] and higher [3] p_T as well as (ii) jet grooming techniques such as filtering [4], pruning [5], and trimming [6], which are designed to improve jet mass resolution. Jet substructure techniques have also been studied in the context of specific particle searches, where they have been shown to substantially extend the reach of traditional search techniques in a wide variety of scenarios, including for example boosted Higgses [4, 7], neutral spin-one resonances [8], searches for supersymmetry [9], and many others [10–14]. Despite these many successes, however, there is every reason to expect that there remains room for refinement of jet substructure techniques.

Top tagging algorithms have reached a mature level of development in recent years [1–3, 15–20]. A variety of different algorithms employ primarily kinematic observables like jet masses and the $W^\pm$ helicity angle in increasingly sophisticated ways, allowing for efficient discrimination between top jets and ordinary QCD jets. One direction that has received less attention is the use of observables that do not map onto the kinematics of hard partons. This article introduces a new non-kinematic observable that can be used in top tagging to gain additional background rejection and should have applications outside of top tagging.

A distinguishing aspect of hadronic top decays is that the jets from the $W^\pm$ decay belong to a color singlet configuration. For $p_{T\,W} \gtrsim m_W$ these jets become close together and will often be clustered within a single jet. The radiation pattern of the $W^\pm$ decay products, which is controlled by the color configuration, has a distinctive form with most of the radiation clustered in between the two jets. This QCD analog of the Chudakov effect offers an additional handle for top discrimination on top of kinematic observables.

The organization of this article is as follows. First the concept of color flow is briefly reviewed, and connection is made to the jet observable pull. Next the proposed "dipolarity" observable is introduced and explored in a general context. Dipolarity is then incorporated into the `HEPTopTagger`, and the performance of the modified tagger is tested on Monte Carlo event samples. Finally, there is some discussion of the results as well as possible applications of dipolarity beyond top tagging.

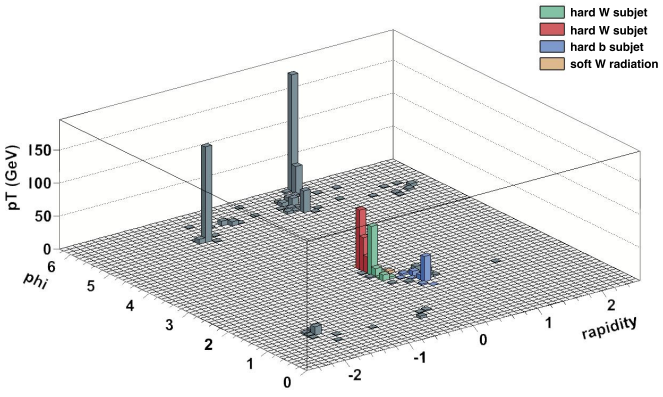

FIG. 1: Legoplot for a top jet reconstructed by the `HEPTopTagger`, with hard substructure identified by a combination of filtering and a fractional mass-drop criterion. The orange cells correspond to soft radiation associated with the $W^\pm$.

Color flow and pull

Within the context of top tagging, several jet observables have been defined that go beyond the kinematics of hard partons. These include a number of jet shape observables such as spherocity [18], planar flow [20, 21], N-subjettiness [22], and template overlap [23]. The jet observable defined in the next section draws from the complimentary information offered by color flow. In a QCD event, radiation is controlled by the kinematics of the hard partons as well as by how color indices are contracted together (color flow). Partons whose color indices are contracted together are color-connected, with a color string stretching between the two color sources. For example, the two quarks in the hadronic decay of a color singlet like the Higgs form a color dipole whose radiation pattern is contained primarily within a pair of cones around the two quarks, with a tendency for more radiation to occur in the region between the two quarks [24].

Color flow arguments of this sort have motivated attempts to use QCD radiation patterns for event discrimination, *e.g.* mini-jet vetoes in Higgs searches [25]. More recently, the authors of [26] introduced a jet observable dubbed pull, which is a p_T-weighted vector in rapidity-phi space that is constructed so as to point from a given jet to its color-connected partner(s). Although pull has been shown to offer some discrimination in particle searches [27], it does not seem well-suited to tagging boosted hadronic tops. The most straightforward way to incorporate pull into a top tagging algorithm is to measure the pull of two subjets that reconstruct the $W^\pm$ and check whether each subjet's pull vector points towards the other subjet. A problem with this approach is that the pull vectors are sensitive to how the $W^\pm$ jet is broken down into two subjets. For a lopsided distribution of the $W^\pm$ into two subjets, one of the subjets will consist of only a small handful of calorimeter cells, and as a consequence its pull will be sensitive to statistical fluctuations and contamination. Even for a $W^\pm$ broken down into two subjets more symmetrically, the pull vectors can depend sensitively on the precise boundary drawn between the two subjets, which itself is a noisy function of the particular jet clustering algorithm being used. A way around these difficulties is to consider the entire radiation pattern of the $W^\pm$ simultaneously. This simple idea leads us to jet dipolarity, which we now define.

Dipolarity

Consider a jet, J, with two subjets, j_1 and j_2, whose centers are located at pseudorapidities η_1 and η_2 and azimuthal angles ϕ_1 and ϕ_2, respectively. For each calorimeter cell $(\eta_i,\, \phi_i)$ with transverse momentum p_{Ti} let R_i be the euclidean distance in the η-ϕ plane between $(\eta_i,\, \phi_i)$ and the line segment that runs from $(\eta_1,\, \phi_1)$ to $(\eta_2,\, \phi_2)$. Dipolarity is defined as the p_T-weighted sum

$$\mathcal{D} \equiv \frac{1}{R_{12}^2} \sum_{i \in J} \frac{p_{Ti}}{p_{T_J}} R_i^2 \tag{1}$$

where $R_{12}^2 \equiv (\eta_1 - \eta_2)^2 + (\phi_1 - \phi_2)^2$. Dipolarity is an infrared and collinear (IRC) safe observable so long as the algorithm used to identify J, j_1 and j_2 is IRC safe. Notice that dipolarity, which is essentially a two-subjet observable, requires the centers of j_1 and j_2 as input, although it does not require that the constituents of J be partitioned between j_1 and j_2. The centers of j_1 and j_2 can be determined by whatever procedure is convenient for the particular application. For example one could choose the centers of j_1 and j_2 so as to minimize the sum in (1).

Dipolarity will be small when most of the radiation within the jet J occurs in the region between the two subjets j_1 and j_2 and will be large whenever a substantial amount of radiation is found elsewhere. As a consequence of the weighting with respect to R_i^2 in (1), $\mathcal{D}$ receives large contributions from semisoft radiation away from the cores of j_1 and j_2. It is this semisoft radiation away from the cores of j_1 and j_2 that is expected to reflect the color configuration of J. The weighting in (1) does not know about the exact radiation pattern of a color singlet; nevertheless, we expect that color singlets that decay into two jets will have small $\mathcal{D}$, while radiation emitted by colored objects will tend to yield larger values of $\mathcal{D}$.

This expectation can be fleshed out more explicitly by considering the emission pattern of a third parton with energy ω from a pair of partons in a particular color configuration, see *e.g.* [24]. In the eikonal approximation ($\omega \to 0$) one finds that for a color singlet

$$W_{\rm s}(\eta, \phi) \sim \frac{d\omega}{\omega} \frac{dy d\phi}{\chi(\eta, \phi; \eta_1, \phi_1)\chi(\eta, \phi; \eta_2, \phi_2)} \tag{2}$$

while for two partons color-connected to the beam

$$W_{\rm ns}(\eta, \phi) \sim \begin{array}{l} \frac{d\omega}{\omega} \\ \\ \frac{d\omega}{\omega} \end{array} \begin{array}{l} \dfrac{d\eta d\phi}{\chi(\eta, \phi; \eta_1, \phi_1)\chi(\eta, \phi; \eta_{\rm beam})} + \\ \\ \dfrac{d\eta d\phi}{\chi(\eta, \phi; \eta_2, \phi_2)\chi(\eta, \phi; \eta_{\rm beam})} \end{array} \tag{3}$$

where

$$\chi(\eta, \phi; \eta_i, \phi_i) \equiv \cosh(\eta - \eta_i) - \cos(\phi - \phi_i) \tag{4}$$

The resulting radiation patterns are depicted in FIG.2. One sees explicitly that the color singlet has its radiation clustered in the region between the two partons, whereas for partons color-connected to the beam, a substantial amount of radiation is emitted towards the beam. Using the expressions in (2) and (3) to calculate $\mathcal{D}$ gives the prediction $\mathcal{D}_{\rm ns} \sim 2\,\mathcal{D}_{\rm s}$; although this is approximately what is found from Monte Carlo calculations, expressions (2) and (3) do not yield dipolarity distributions in quantitative agreement with the Monte Carlo. Given the crudeness of the approximations that went into these expressions, this discrepancy is not surprising; a more accurate

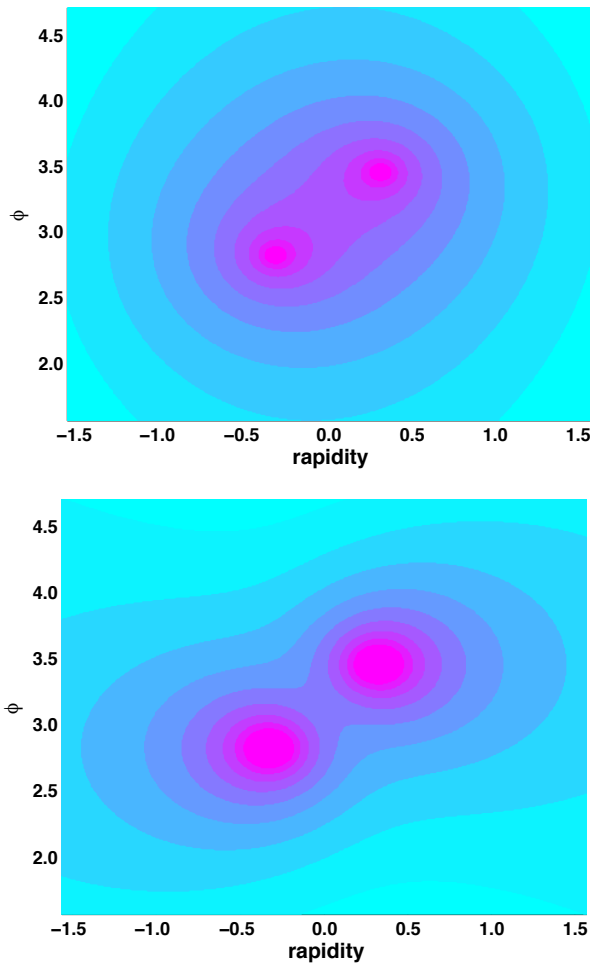

FIG. 2: Top: Eikonal radiation pattern $dp_T/d\eta d\phi$ for a color singlet with ΔR=0.9, typical for a $W^\pm$ originating from a top with $p_T \sim 300$ GeV. Bottom: As above with the partons instead color-connected to the beam (left/right-going parton connected to the left/right beam). For the color singlet the radiation is mostly found in the region between the two subjets. For the background-like color configuration, the radiation is pulled towards the beam. See (2) and (3).

estimate of $\mathcal{D}$ for various color configurations could be obtained by using antenna patterns as in [28].

Dipolarity can be used within the context of top tagging to reduce QCD backgrounds. Consider a collection of fat QCD jets originating from parton branchings with identical kinematics but different color configurations as illustrated in FIG. 3. If one of the QCD jets fakes the kinematics of a top quark decay, then each of the different color configurations fakes the kinematics equally well. The dipolarities of the subjets, however, will be broadly distributed in accord with their different color configurations. For instance, gluon jets are known to give the largest fake rates for top jets as a consequence of their larger Casimirs which more often result in wide angle branchings with significant mass drops. FIG. 3 illustrates how gluon jets, with their distinct color configurations,

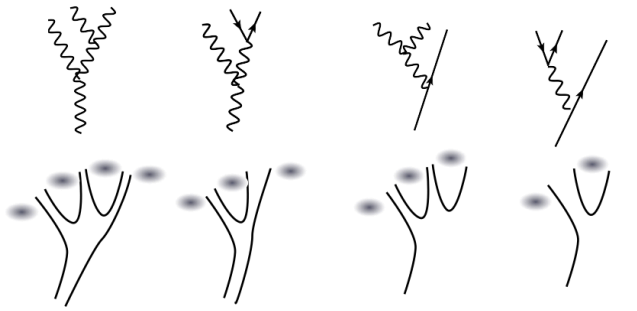

FIG. 3: Schematic for a collection of QCD jets whose kinematics fake the top. The upper figures show various possibilities for quarks and gluons that undergo two branchings. The bottom figures show the corresponding large N_c color diagrams, with dipole radiation patterns superimposed across color dipoles. Only the rightmost color configuration, which is suppressed by factors of C_A/C_F with respect to the others, matches the radiation pattern of an actual top.

radiate differently from top jets. All of this suggests that the dipolarity of the $W^\pm$ in a hadronic top decay is well-suited as a discriminant in top tagging algorithms.

`HEPTopTagger`

To test whether dipolarity makes an effective discriminant, cuts on dipolarity are incorporated into the `HEPTopTagger` [1, 2], which is designed to work effectively at intermediate boost, with $200\,\text{GeV} \lesssim p_T \lesssim 800\,\text{GeV}$. The high efficiency of the `HEPTopTagger` at these p_T makes it a good candidate for such a modification because dipolarity cuts are expected to be most effective at intermediate p_T. This is because at lower p_T contamination from pile-up and the underlying event becomes more of a concern as the top jets become fatter and fatter, while at higher p_T the finite resolution of the detector makes it difficult to get an accurate handle on radiation patterns. Furthermore, the multibody filtering implemented by the `HEPTopTagger` results in accurate reconstruction of the $W^\pm$. The `HEPTopTagger` algorithm is defined as follows.[1]

1. Using the Cambridge/Aachen algorithm cluster the event into fat $R = 1.5$ jets.

2. Break each fat jet into hard subjets using the following mass-drop criterion. Undo the last stage of clustering to yield two subjets j_1 and j_2 (with $m_{j_1} > m_{j_2}$), keeping both j_1 and j_2 if $m_{j_1} < 0.8 m_{j_2}$

[1] The `HEPTopTagger` does not make use of b-tagging, which is a natural extension to the algorithm that can result in significant improvements in background rejection. Since dipolarity cuts are orthogonal to b-tagging, we do not explore the use of b-tagging in this paper.

and otherwise dropping j_2. Repeat this procedure recursively, stopping when the m_{j_i} drop below 30 GeV.

3. Consider in turn all possible triplets of hard subjets. First, filter each triplet with a resolution $R_{\rm filter} = \min(0.3, \Delta R_{ij}/2)$. Next, using the five hardest constituent subjets of the filtered triplet calculate the jet mass $m_{\rm filt}$. Finally, choose the triplet whose $m_{\rm filt}$ lies closest to m_t.

4. Recluster the five filtered constituents chosen in step 3 into exactly three subjets j_1, j_2, and j_3 ordered in descending p_T. Accept the fat jet as a top candidate if it passes any of the following three pairs of mass cuts:

i) $0.2 \leq \arctan m_{13} \leq 1.3$

i′) $R_{\rm min} \leq \dfrac{m_{23}}{m_{123}} \leq R_{\rm max}$

ii) $R^2_{\rm min}\left(1+\dfrac{m^2_{13}}{m^2_{12}}\right) \leq 1 - \dfrac{m^2_{23}}{m^2_{123}} \leq R^2_{\rm max}\left(1+\dfrac{m^2_{13}}{m^2_{12}}\right)$

ii′) $\dfrac{m_{23}}{m_{123}} \geq 0.35$

iii) $R^2_{\rm min}\left(1+\dfrac{m^2_{12}}{m^2_{13}}\right) \leq 1 - \dfrac{m^2_{23}}{m^2_{123}} \leq R^2_{\rm max}\left(1+\dfrac{m^2_{12}}{m^2_{13}}\right)$

iii′) $\dfrac{m_{23}}{m_{123}} \geq 0.35$

Here $R_{\rm min} = 85\% \times m_W/m_t$ and $R_{\rm max} = 115\% \times m_W/m_t$.

5. Finally, require that the total p_T of the three subjets defined in step 4 be greater than 200 GeV.

Dipolarity cuts are introduced into the `HEPTopTagger` by modifying step 4 above. For a top candidate that has passed one of the three pairs of mass cuts we calculate the dipolarity of the $W^\pm$ as identified by the mass cut: *e.g.* for a top candidate that satisfies ii) and ii') the $W^\pm$ is identified as j_1+j_2. If more than one of the pairs of mass conditions is satisfied in step 4, we choose the smaller dipolarity. We find that this procedure performs better than calculating the dipolarity of the pair of subjets that reconstructs m_W most accurately.

In addition to introducing dipolarity cuts, we also make cuts on the filtered mass of the reconstructed top, $m_{\rm filt}$, which is not done in the original `HEPTopTagger`, where the cuts have been chosen so as to avoid any explicit mass scales. We introduce cuts on $m_{\rm filt}$ for two reasons. The first is to improve background rejection. The second and main reason is that we are interested in determining whether dipolarity cuts are essentially orthogonal to cuts on kinematic observables. To do this we must ensure that the `HEPTopTagger` is using a full compliment of kinematic cuts, including cuts on $m_{\rm filt}$. In a particular application, cuts on $m_{\rm filt}$ may be undesirable. In that case, the inclusion of dipolarity cuts would result in a larger improvement of background rejection.

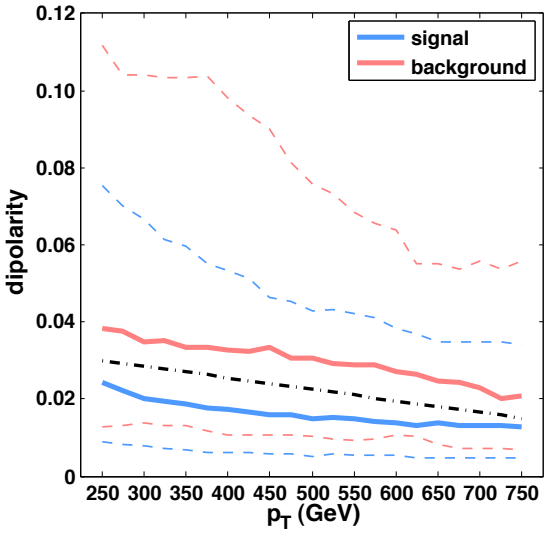

FIG. 4: Dipolarity distributions for $W^\pm$s reconstructed by the `HEPTopTagger` and passing default mass cuts with $m_{\rm filt} \in$ [150 GeV, 210 GeV]. Thick solid lines indicate central values, whereas thin dashed lines correspond to values at 10% and 90%. Here and throughout the p_T is that of the fat $R = 1.5$ jet. For all p_T the central value of the dipolarity for the background is $\mathcal{O}(50\% - 100\%)$ larger than for the signal. This figure uses the `HERWIG` event samples; the `PYTHIA` event samples yield similar distributions. The dot-dash line roughly indicates where dipolarity cuts are made at the S=20% working point.

Note that the j_i selected in step 4 contain only the hard substructure of the fat jet. Some amount of soft radiation has been thrown out by filtering and the mass drop criterion. To effectively gauge whether the radiation pattern of the reconstructed $W^\pm$ is consistent with the expected dipole radiation pattern, it is important to include some of the discarded soft radiation. We find that the criterion used to select the radiation included in calculating the dipolarity of the $W^\pm$ has significant impact on the ultimate utility of dipolarity as a discriminant. In particular different criteria will lead to dipolarity distributions that are more or less correlated with the kinematic observables considered by the `HEPTopTagger`. Applying dipolarity in another context would likely require this criterion to be carefully reworked so as to maximize performance. In the present case we find that the following criterion, which aims to capture as much of the radiation emitted by the $W^\pm$ as possible, while minimizing possible contamination, to be most effective. In addition to the hard radiation from the two $W^\pm$ subjets, we include all soft radiation contained within the pair of cones centered around the two hard $W^\pm$ subjets, fixing the radius of the cones to be $\Delta R/\sqrt{2}$, where ΔR is defined between the two hard $W^\pm$ subjets. Furthermore we exclude any radiation contained within the smallest cone that encloses the hard b subjet. Note that angular ordering implies that the majority of the radiation emitted by the $W^\pm$

is within the pair of cones of radius ΔR. We choose our cones to be somewhat smaller to minimize contamination from underlying event/pile-up as well as the b subjet.

Testing Dipolarity

In order to make a meaningful comparison between the performance of the `HEPTopTagger` with and without dipolarity cuts, it is not enough to leave the kinematic cuts employed by the `HEPTopTagger` fixed at their default values. Instead it is important to optimize the cuts to yield the largest background rejection at each given signal efficiency. This optimization is performed by a custom Monte Carlo code that finely samples the space of cuts. Specifically, a scan is performed at discrete values of $R_{\rm min}$

$$70\%\ m_W/m_t \leq R_{\rm min} \leq 98\%\ m_W/m_t$$

with step sizes of $1\%\ m_W/m_t$. For each value of $R_{\rm min}$, $R_{\rm max}$ is chosen to be $R_{\rm max} = 2.0 \times m_W/m_t - R_{\rm min}$. In addition we simultaneously optimize over cuts $m_{t\ \rm min} \leq m_{\rm filt} \leq m_{t\ \rm max}$, $\mathcal{D} \leq \mathcal{D}_{\rm max}$, and, in step 4 of the `HEPTopTagger`, $l_{\rm cut} \leq \arctan m_{13}$ and $b_{\rm cut} \leq m_{23}/m_{123}$. The remaining cuts in step 4 of the `HEPTopTagger` are left at their default values, since these are less important for background rejection. Additionally, the two parameters that define the mass drop criterion remain fixed at their default values. The hard substructure cutoff of 30 GeV is sensitive to detector effects, which can only be crudely mocked-up without a full detector simulation.

We use three different event samples for evaluating the performance of the modified `HEPTopTagger`. These event samples (with center of mass energy of 7 TeV) belong to a set of benchmark event samples that have been made publicly available by participants of BOOST 2010 [29]. The first event sample is generated by `HERWIG` 6.510 [30] with the underlying event simulated by `JIMMY` [31], which has been configured with a tune used by ATLAS. The second is generated by `PYTHIA` 6.4 [32] with Q^2-ordering and the 'DW' tune for the underlying event. The third is generated by `PYTHIA` 6.4 [32] with p_T-ordering and the 'Perugia' tune for the underlying event. See [33] for more details. For signal jets we use the hardest jet in each event of a Standard Model hadronic $t\bar{t}$ sample, excluding jets with $|\eta| > 2.5$. For background jets we use the hardest jet in each event of a Standard Model dijet sample, again excluding jets with $|\eta| > 2.5$. For jet clustering we use the Cambridge-Aachen (CA) algorithm [34, 35] as implemented by `FastJet 2.4.2` [36]. In order to simulate the finite resolution of the ATLAS or CMS calorimeters, particles in each event are clustered into 0.1×0.1 cells in $\eta - \phi$ space and then combined into massless four-vector pseudoparticles that are fed into `FastJet`. We have also checked that imposing a low energy cutoff of 1 GeV on each cell results in only a mild degradation of background rejection.

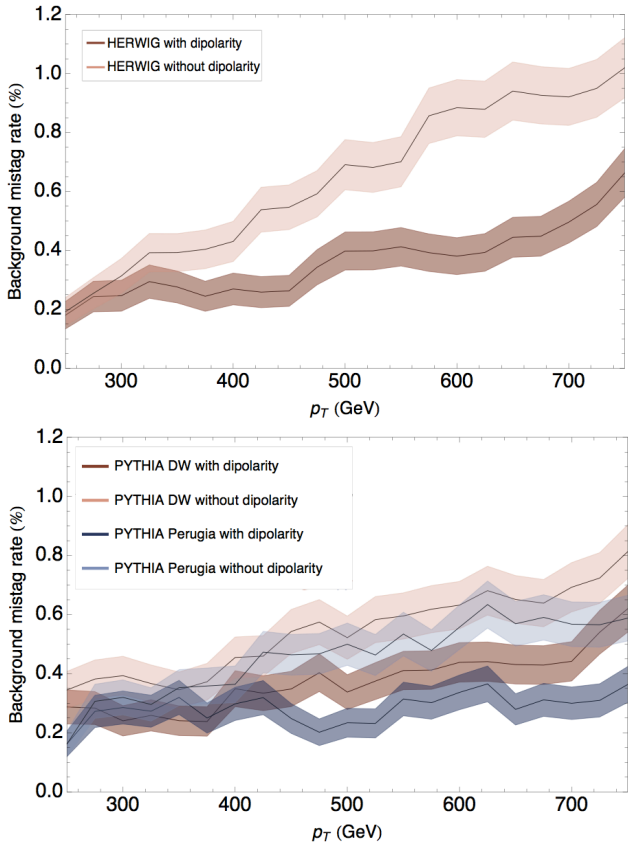

FIG. 5: Background mistag rates with and without dipolarity cuts at a fixed signal efficiency of 20% for `HERWIG` (top) and `PYTHIA` (bottom). The mistag rate at a given p_{T0} is calculated from a p_T window of 100 GeV centered at p_{T0}. Note that, as a consequence, each point is not statistically independent. Error bands are statistical.

FIG. 5 shows the improvement in performance that results from including dipolarity cuts into the `HEPTopTagger` at a fixed signal efficiency of $S = 20\%$. Dipolarity cuts lead to a sizable decrease in the mistag rate for $350\,\text{GeV} \lesssim p_T \lesssim 800\,\text{GeV}$ with the largest decrease at intermediate p_T. For the `HERWIG` event samples the mistag rate decreases by as much as $\sim 50\%$, whereas for the `PYTHIA` samples the mistag rate decreases by a more modest amount, $\sim 30\%$. Differences in the underlying event (UE) model do not explain this disagreement; for instance, repeating the analysis with the UE turned off results in background mistag rates that are only somewhat smaller, with both `HERWIG` and `PYTHIA` dropping by similar amounts. This suggests that the difference between the `HERWIG` and `PYTHIA` mistag rates most likely arises from the parton shower.

Discussion

This article has introduced a new jet substructure observable that is useful in discriminating among different

Operating Point	$l_{\rm cut}$	$b_{\rm cut}$	$r_{\rm min}$	$\mathcal{D}_{\rm max}$	$m_{t\ \rm min}$	$m_{t\ \rm max}$	B (%)		
Low p_T without $\mathcal{D}$ cut	0.45	0.41	0.92	-	159 GeV	195 GeV	0.47	0.48	0.41
Low p_T with $\mathcal{D}$ cut	0.37	0.39	0.80	0.021	154 GeV	199 GeV	0.41	0.38	0.30
High p_T without $\mathcal{D}$ cut	0.47	0.40	0.93	-	158 GeV	199 GeV	0.92	0.79	0.59
High p_T with $\mathcal{D}$ cut	0.36	0.38	0.88	0.023	154 GeV	196 GeV	0.58	0.58	0.39

TABLE I: Sample optimized operating points at $S = 20\%$ based on an equal admixture of all three event samples for maximum statistics. The resulting background mistag rates (B) are shown for each of the three event samples with `HERWIG`, `PYTHIA` 'DW', and `PYTHIA` 'Perugia' arranged from left to right. Including dipolarity cuts loosens mass cuts while improving background rejection. The low p_T samples have $200\,\text{GeV} \leq p_T \leq 500\,\text{GeV}$ while the high p_T samples have $400\,\text{GeV} \leq p_T \leq 800\,\text{GeV}$.

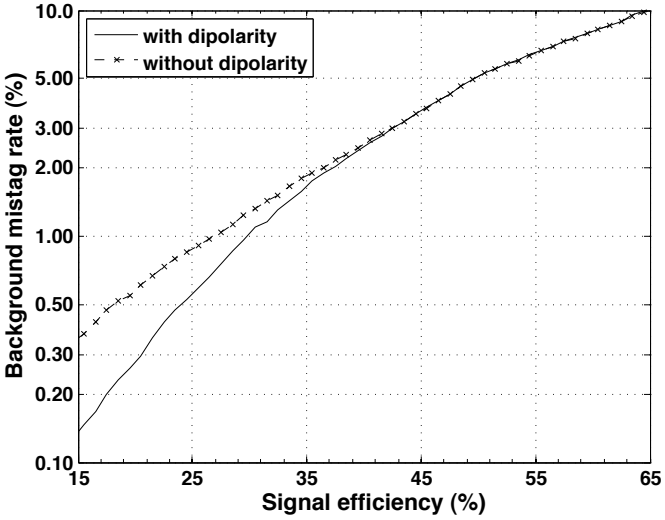

FIG. 6: Signal efficiency vs. background mistag rate for the `HEPTopTagger` with $p_T \in [400\,\text{GeV}, 500\,\text{GeV}]$ and `HERWIG` event samples. At lower signal efficiencies the inclusion of dipolarity cuts leads to a sizeable improvement in background rejection. Statistical error bars, which are a relative 25% at the lowest mistag rate, are not shown.

color configurations in jets that have large mass drops. This discrimination is of interest, since such jets often arise from decays of boosted heavy particles. Incorporating this discriminant into a top tagging algorithm results in QCD background mistag rates that are lower by as much as 50%; the exact mistag rate, however, shows considerable sensitivity to the details of the parton shower. Specifically `HERWIG` event samples result in a larger improvement in background rejection than is found for `PYTHIA`. We suspect that `HERWIG`, which uses angular ordering, does a better job of simulating the effects of color coherence than `PYTHIA`, which uses Q^2 or p_T-ordering in combination with angular vetoes. This could explain why the dipolarity of the $W^\pm$ is a more discriminating observable in the case of the `HERWIG` event samples. With an understanding of the origin of this difference, comparisons to measurements at the LHC could help improve the description of QCD radiation. It would be interesting to understand how this difference arises from the details of the parton shower; doing so, however, lies outside the scope of this paper.

Validating how well color flow effects as modeled by Monte Carlo event generators match what is observed in collider experiments is only beginning to be studied actively. Understanding color flow in detail is a difficult problem; for example, QCD predictions for radiation patterns can be affected by non-global logarithms, see *e.g.* [40]. Therefore validating theoretical predictions against data will be critical in reducing the theoretical uncertainty associated with how dipolarity and other color flow observables are modeled by Monte Carlo calculations. A few color coherence studies performed at the Tevatron showed spatial correlations between the third and second hardest jets in $p\bar{p}$ collisions, and `HERWIG` was shown to provide a better description of the data than `PYTHIA` [37]. More recently, the color of the $W^\pm$ in $t\bar{t}$ events was studied, and agreement between theory predictions for jet pull and data was shown [38].

Jet dipolarity should be useful in a broader set of applications to both Standard Model and beyond the Standard Model physics. Possible directions for future research include: (i) applications of dipolarity to a collider search for heavy color singlet resonances that decay to $t\bar{t}$; (ii) applications to standard model $W^\pm/Z^0$ physics; (iii) applications to heavy color singlet resonances that decay to W^+W^- or Z^0Z^0; (iv) applications to cascade decays of supersymmetric particles; (v) inclusion of dipolarity into other top-tagging algorithms; (vi) applications to the decay of new particles into novel color configurations such as in the decay of the LSP in supersymmetric models with baryonic R-parity violation; and (vii) modifying $\mathcal{D}$ to more closely correspond to the exact radiation pattern of a color singlet. Each of these directions could make an interesting laboratory for further development of jet substructure techniques.

Acknowledgements

We would like to thank Maria Baryakhtar for collaboration at early stages of this work. We would also like to thank Tilman Plehn, Gavin Salam and Michael Spannowsky for providing us with their implementation of the

HEPTopTagger. JW would like to thank Tilman, Plehn, Gavin Salam, and David E. Kaplan for useful conversations during the course of this work. MJ would like to thank Jason Gallicchio for interesting conversations about color pull. MJ, AH and JGW are supported by the US DOE under contract number DE-AC02-76SF00515. MJ, AH and JGW receive partial support from the Stanford Institute for Theoretical Physics. JGW is partially supported by the US DOE's Outstanding Junior Investigator Award and the Sloan Foundation.

[1] T. Plehn, G. P. Salam, M. Spannowsky, Phys. Rev. Lett. **104**, 111801 (2010) [arXiv:0910.5472].
[2] T. Plehn, M. Spannowsky, M. Takeuchi and D. Zerwas, JHEP **1010**, 078 (2010) [arXiv:1006.2833].
[3] D. E. Kaplan, K. Rehermann, M. D. Schwartz and B. Tweedie, Phys. Rev. Lett. **101**, 142001 (2008) [arXiv:0806.0848].
[4] J. M. Butterworth, A. R. Davison, M. Rubin and G. P. Salam, AIP Conf. Proc. **1078**, 189 (2009) [arXiv:0809.2530]. J. M. Butterworth, A. R. Davison, M. Rubin and G. P. Salam, Phys. Rev. Lett. **100**, 242001 (2008) [arXiv:0802.2470].
[5] S. D. Ellis, C. K. Vermilion and J. R. Walsh, Phys. Rev. D **81**, 094023 (2010) [arXiv:0912.0033].
[6] D. Krohn, J. Thaler, L. -T. Wang, JHEP **1002**, 084 (2010). [arXiv:0912.1342]
[7] C. Hackstein and M. Spannowsky, [arXiv:1008.2202].
[8] A. Katz, M. Son, and B. Tweedie, [arXiv:1010.5253].
[9] G. D. Kribs, A. Martin, T. S. Roy and M. Spannowsky, Phys. Rev. D **82**, 095012 (2010) [arXiv:1006.1656].
[10] C. R. Chen, M. M. Nojiri and W. Sreethawong, JHEP **1011** (2010) 012 [arXiv:1006.1151].
[11] A. Falkowski, D. Krohn, L. T. Wang, J. Shelton and A. Thalapillil, [arXiv:1006.1650].
[12] G. D. Kribs, A. Martin, T. S. Roy and M. Spannowsky, Phys. Rev. D **81**, 111501 (2010) [arXiv:0912.4731].
[13] J. M. Butterworth, J. R. Ellis, and A. R. Raklev, *JHEP* **05** (2007) 033, [hep-ph/0702150].
[14] C. Englert, C. Hackstein, and M. Spannowsky, [arXiv:1010.0676].
[15] G. Brooijmans, **ATL-PHYS-CONF-2008-008**.
[16] **CMS** Collaboration, R. Adolphi *et al.*, *CMS Physics Analysis Summary* **CMS-PAS-JME-09-001** (2009).
[17] M. Vos, ATL-PHYS-CONF-2008-016.
[18] J. Thaler and L.-T. Wang, *JHEP* **07** (2008) 092, [arXiv:0806.0023].
[19] K. Rehermann and B. Tweedie, arXiv:1007.2221.
[20] L. G. Almeida, S. J. Lee, G. Perez, I. Sung and J. Virzi, Phys. Rev. D **79**, 074012 (2009) [arXiv:0810.0934].
[21] L. G. Almeida, S. J. Lee, G. Perez, G. F. Sterman, I. Sung and J. Virzi, Phys. Rev. D **79**, 074017 (2009) [arXiv:0807.0234].
[22] J. Thaler and K. Van Tilburg, [arXiv:1011.2268].
[23] L. G. Almeida, S. J. Lee, G. Perez, G. Sterman and I. Sung, Phys. Rev. D **82**, 054034 (2010) [arXiv:1006.2035].
[24] A. Bassetto, M. Ciafaloni, G. Marchesini, Phys. Rept. **100**, 201-272 (1983); R. K. Ellis, W. J. Stirling, B. R. Webber, "QCD and collider physics," Camb. Monogr. Part. Phys. Nucl. Phys. Cosmol. **8**, 1-435 (1996); and also references therein.
[25] V. D. Barger, R. J. N. Phillips and D. Zeppenfeld, Phys. Lett. B **346**, 106 (1995) [arXiv:9412276].
[26] J. Gallicchio and M. D. Schwartz, Phys. Rev. Lett. **105**, 022001 (2010) [arXiv:1001.5027].
[27] K. Black, J. Gallicchio, J. Huth, M. Kagan, M. D. Schwartz and B. Tweedie, [arXiv:1010.3698].
[28] A. J. Larkoski and M. E. Peskin, Phys. Rev. D **81**, 054010 (2010) [arXiv:0908.2450].
[29] Events are located at http://www.lpthe.jussieu.fr/∼salam/projects/boost2010-events/ http://tev4.phys.washington.edu/TeraScale/boost2010/
[30] HERWIG 6.5, G. Corcella, I.G. Knowles, G. Marchesini, S. Moretti, K. Odagiri, P. Richardson, M.H. Seymour and B.R. Webber, JHEP 0101 (2001) 010 [arXiv:0011363]; [arXiv:0210213].
[31] J. M. Butterworth, J. R. Forshaw, and M. H. Seymour, Multiparton interactions in photoproduction at HERA, Z. Phys. C72 (1996) 637646, [arXiv:9601371].
[32] T. Sjostrand, S. Mrenna, and P. Z. Skands, PYTHIA 6.4 Physics and Manual, JHEP 05 (2006) 026, [arXiv:0603175].
[33] A. Abdesselam *et al.*, [arXiv:1012.5412].
[34] Y. L. Dokshitzer, G. D. Leder, S. Moretti and B. R. Webber, JHEP **9708**, 001 (1997) [arXiv:9707323].
[35] M. Wobisch and T. Wengler, [arXiv:9907280].
[36] M. Cacciari and G. P. Salam, Phys. Lett. B **641**, 57 (2006) [arXiv:0512210]. M. Cacciari, G.P. Salam and G. Soyez, http://fastjet.fr/
[37] F. Abe *et al.* [CDF Collaboration], Phys. Rev. D **50**, 5562 (1994). B. Abbott *et al.* [D0 Collaboration], Phys. Lett. B **414**, 419 (1997) [arXiv:9706012]. N. Varelas [arXiv:9809019].
[38] V. M. Abazov *et al.* [D0 Collaboration], Submitted to: Phys.Rev.Lett. [arXiv:1101.0648].
[39] D. L. Rainwater, R. Szalapski, D. Zeppenfeld, Phys. Rev. **D54**, 6680-6689 (1996). [arXiv:9605444].
[40] M. Dasgupta, Pramana **62**, 675 (2004) [arXiv:0304086].